Journal of Electroceramics 3:3, 233–238, 1999

Doping Mechanism and Permittivity Correlations in Nd-Doped $BaTiO_3$

N. HIROSE, J.M.S. SKAKLE & A.R. WEST*
University of Aberdeen, Department of Chemistry, Meston Walk, Aberdeen AB24 3UE

Submitted September 23, 1998; Revised December 17, 1998; Accepted December 17, 1998

Abstract. $BaTiO_3$ forms an extensive range of solid solutions with Nd_2O_3 by means of the double substitution mechanism: Ba + Ti ⇒ 2Nd, as shown by both a phase diagram study and Rietveld refinement using powder neutron diffraction data. The solid solutions have the general formula $Ba_{1-x}Ti_{1-x}Nd_{2x}O_3$: $O \leq x \leq 0.12$ at 1300°C and $0 \leq x \leq 0.14$ at 1400°C. With increasing x, the symmetry changes from tetragonal to cubic at $x \sim 0.09$. The sharp permittivity maximum at ~127°C in stoichiometric $BaTiO_3$ broadens very rapidly with increasing x and gradually moves to lower temperatures: this appears to be because, with substitution of Nd onto Ti sites, formation of the ferroelectric domains is increasingly difficult because of the presence of dipole-inactive Nd^{3+} ions on the Ti sites.

Keywords: Barium titanate, permittivity, phase diagram

Introduction

In spite of an enormous amount of research into the science and technological development of barium titanate ceramics for capacitor and PTCR (positive temperature coefficient of resistance) applications, many fundamental questions over the structure and properties of $BaTiO_3$ remain. For instance, for PTCR devices, it is well-established that doping with a small amount of a large trivalent element, such as *Y* or a rare earth, changes the electrical properties from insulating to semiconducting. With larger concentrations of ''donor'' dopant, however, a return to insulating behavior occurs. This indicates that both electronic and ionic compensation mechanisms operate on doping $BaTiO_3$ with large trivalent ions.

Various ionic compensation mechanisms have been proposed in the literature with, in many cases, little direct evidence in favor of a particular mechanism. Recently, we have confirmed [1] by means of a systematic phase diagram study, in parallel with neutron diffraction, that in the case of doping $BaTiO_3$ with La, a Ti vacancy mechanism [2] is predominant:

$$4Ba^{II} + Ti^{IV} \Rightarrow 4La^{III} + V_{Ti}$$

These studies were made possible because the solid solutions extend over a wide composition range. However, in cases where the degree of doping is very limited, it can be difficult to ascertain the precise mechanism due to the insensitivity of crystallographic techniques to small departures from stoichiometry. Our approach is, therefore, to investigate more heavily-doped materials, and where possible extrapolate the behavior, structure and properties to those expected at lower dopant levels. For this, it is necessary first to determine the relevant phase diagram, which should give the locus of any solid solution region and hence, an indicator of the most probable doping mechanism. This is then combined with crystallographic studies on materials with high dopant concentrations.

As far as we are aware, systematic, multi-technique approaches to phase diagrams, crystal structures and

*Currently at Sheffield University, Department of Engineering Materials, Mappin St, Sheffield S1 3JD

properties of doped barium titanate have not been reported, although many studies of individual aspects have been made. Many dielectric studies of heavily-doped $BaTiO_3$ have been reported [3–8] which were usually related to the microstructure of the products, rather than to the substitution mechanism. A reconnaissance study of subsolidus relations in the system BaO-Nd_2O_3-TiO_2 established the most extensive region of solid solution formation as lying on the join $BaTiO_3$-Nd_2O_3 [9] although other studies had found extensive solid solutions instead on other joins [10–11]; in this work, we report the results of a detailed study of the stoichiometry, structure, and electrical properties of the $BaTiO_3$ solid solutions on the join $BaTiO_3$—Nd_2O_3.

Experimental

Reagents used were high purity $BaCO_3$, Nd_2O_3 and TiO_2, which were dried prior to weighing. Samples in ca. 10 g amounts were mixed with an agate mortar and pestle using acetone to form a paste, dried and fired in platinum boats, initially at 800 to 900°C for 6 h to expel CO_2 and then at 1100 to 1400°C for 2–3 days, with intermediate regrinding, to complete the reaction. For phase identification, a Philips Hagg Guinier powder X-ray diffraction (XRD) camera was used, and for accurate lattice parameters, a Stoe StadiP XRD system, CuKα_1 radiation, with a small, linear, position sensitive detector. The Stoe diffractometer was calibrated using a silicon external standard.

For crystallographic studies, powder neutron diffraction data were recorded using the Polaris diffractometer at the ISIS facility, Rutherford Appleton Laboratory. Structures were refined using the program TF14LS [12,13] using data collected over the time-of-flight range 2200–19500 μs in the highest resolution, backscattering detectors. For impedance measurements, pressed pellets were sintered at 1250°C, 72 h and 1300°C, 2 h; some pellets were additionally heated at 1350°C. Electrodes were fabricated from liquid In/Ga alloy which was brushed onto the pellet faces; pellets were connected, via Au foil strips, to the Pt leads of a conductivity jig which was mounted inside a horizontal tube furnace whose temperature was controlled and measured to within 1 degree. Impedance data were recorded on a stepwise heating cycle using Solartron 1250/1286 instrumentation over the frequency range 100 mHz to 64 kHz; fixed frequency permittivities, at 1 kHz, were extracted from the impedance data. A few measurements were made on a stepwise cooling cycle to confirm the reproducibility and reversibility of the data. Electron-probe microanalysis (EPMA) was performed on pelleted samples using a Cameca SX51 EPMA, with NdF_3 and $BaTiSi_3O_9$ (Microanalysis Consultants) as standards.

Results and Discussion

A series of compositions with general formula $Ba_{1-x}Nd_{2x}Ti_{1-x}O_3$ was synthesized. From the XRD results, single phase solid solutions were found to form over the range $0 < x < 0.12(1)$ at 1300°C extending to $0 \leq x \leq 0.14$ at 1400°C. Figure 1 shows the variation of lattice parameters with composition for samples quenched from 1350°C; at low x, $< 0.09(1)$, the samples are tetragonal; at higher x, they are cubic. Samples with $x = 0.06, 0.08$, quenched from 1350°C had broad X-ray peaks and intensities were low. This suggests the coexistence of tetragonal and cubic phases which is associated with a diffuse cubic-tetragonal phase transition and is commonly observed in $BaTiO_3$ solid solutions [8,14–17].

Samples with $x > 0.12$ heated at 1250°C contained $BaTiO_3$ solid solution and Nd_2O_3; heat treatment at 1300 and 1400°C gave single phase $BaTiO_3$ solid solution for $x = 0.12$ and 0.14, respectively, but for $x = 0.16$ the Nd_2O_3 second phase persisted up to the melting temperature of ca. 1450°C. On re-annealing single phase samples of $x = 0.12$ and 0.14 at 1250 and

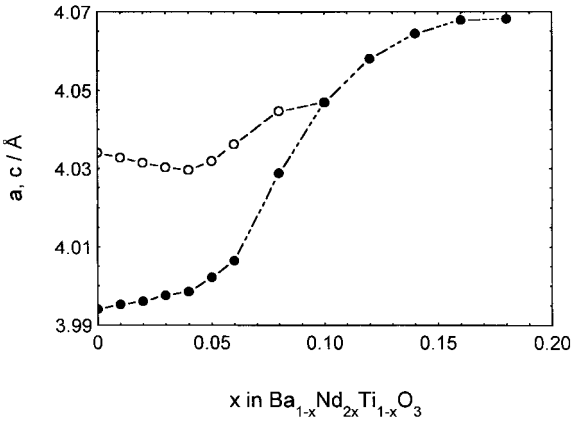

Fig. 1. Lattice parameters vs. composition.

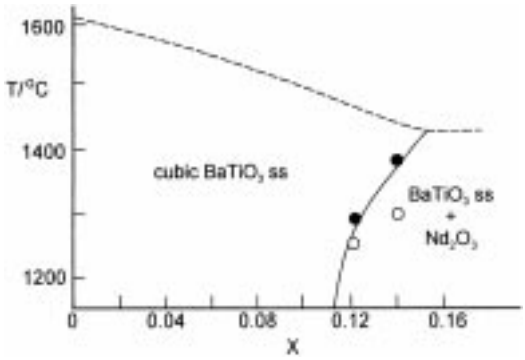

Fig. 2. Phase diagram of the $BaTiO_3$ solid solutions.

1300°C, respectively, small amounts of second phase reappeared. Hence, the solid solution limit is temperature dependent and increases from $x = 0.12(2)$ at 1300°C to 0.14(1) at 1400°C; Fig. 2 shows an approximate binary phase diagram for this system based on the above results.

The solid solution compositions and the solid solution limit at 1400°C were confirmed by EPMA analysis, Table 1. There is excellent agreement between expected and analyzed compositions for $0 \leq x \leq 0.14$ but for $x = 0.16$ the analyzed composition indicates the solid solution limit to be $x \cong 0.14$ at this temperature. Thus, the determined solid solution range is in good agreement with the result of Zheng et al. [9] but more extensive than that of Shaikh et al. [11] who gave a limit of $x = 0.06$. By EPMA, composition $x = 0.16$ contained small amounts of both Nd_2O_3 and Nd_2TiO_5 as extra phases. The occurrence of the latter is attributed to a small amount of BaO loss, probably by reaction with the Pt container, during firing, and is consistent with the subsolidus phase diagram which shows the compatibility triangle $BaTiO_3$ss$+Nd_2O_3 + Nd_2TiO_5$ [9].

Neutron diffraction data for one composition in the cubic range, $x = 0.10$, were collected and the structure refined using the atomic coordinates of the cubic perovskite structure as starting parameters. The overall stoichiometry was fixed, according to $x = 0.1$. The cation site occupancies were varied, with Ba, Nd on A-sites and Ti, Nd on B-sites. Isotropic temperature factors for the two cation sites and anisotropic temperature factors for oxygen were refined. The refinement results, Table 2, showed an equipartitioning of Nd over both A and B sites, thus confirming the correctness of the proposed substitution mechanism for the solid solutions. An alternative model was tested in which the sites were again constrained to be fully occupied but the overall composition was allowed to vary. No significant improvement in *R*-factors was obtained and the refined stoichiometry was still within two esd's of the nominal composition. The difference profile after refinement is shown in Fig. 3.

This substitution mechanism: $Ba + Ti \Leftrightarrow 2Nd$, is clearly different from that of La-doped $BaTiO_3$: $4Ba + Ti \Leftrightarrow 4La + V_{Ti}$, in which La substitutes onto the Ba site with concomitant creation of Ti vacancies [2]. Nd and La are both large rare earths, but whereas the ionic radius of Nd is almost exactly midway between those of Ti and Ba, La is slightly larger. Thus, Nd appears to substitute equally well at both Ba and Ti sites, whereas La appears to substitute exclusively at the Ba site.

Table 1. EPMA results for compositions in the solid solutions $Ba_{1-x}Nd_{2x}Ti_{1-x}O_3$ heated at 1400°C. Oxygen was not directly analyzed, but was calculated by difference

x	Nominal composition	Analyzed atom% Ba	Nd	Ti	O	Phase composition
0.005	$Ba_{0.995}Nd_{0.01}Ti_{0.995}O_3$	19.87(15)	0.19(12)	19.92(16)	60.02(38)	$Ba_{0.994(8)}Nd_{0.010(6)}Ti_{0.996(8)}O_{3.001(19)}$
0.01	$Ba_{0.99}Nd_{0.02}Ti_{0.99}O_3$	19.77(21)	0.37(15)	19.79(24)	60.07(48)	$Ba_{0.989(11)}Nd_{0.019(8)}Ti_{0.990(12)}O_{3.00(2)}$
0.02	$Ba_{0.98}Nd_{0.04}Ti_{0.98}O_3$	19.62(23)	0.82(15)	19.63(17)	59.93(47)	$Ba_{0.981(12)}Nd_{0.041(8)}Ti_{0.982(9)}O_{3.00(2)}$
0.04	$Ba_{0.96}Nd_{0.08}Ti_{0.96}O_3$	19.15(31)	1.55(17)	19.24(23)	60.06(52)	$Ba_{0.958(16)}Nd_{0.078(8)}Ti_{0.962(12)}O_{3.00(3)}$
0.06	$Ba_{0.94}Nd_{0.12}Ti_{0.94}O_3$	18.87(25)	2.44(15)	18.83(28)	59.86(51)	$Ba_{0.944(13)}Nd_{0.122(8)}Ti_{0.942(14)}O_{2.99(2)}$
0.08	$Ba_{0.92}Nd_{0.16}Ti_{0.92}O_3$	18.43(18)	3.12(21)	18.36(22)	60.09(50)	$Ba_{0.922(9)}Nd_{0.156(11)}Ti_{0.918(11)}O_{3.00(3)}$
0.10	$Ba_{0.90}Nd_{0.20}Ti_{0.90}O_3$	17.94(24)	4.10(17)	18.08(19)	59.88(48)	$Ba_{0.897(12)}Nd_{0.205(9)}Ti_{0.904(10)}O_{2.99(2)}$
0.12	$Ba_{0.88}Nd_{0.24}Ti_{0.88}O_3$	17.66(27)	4.77(18)	17.61(25)	59.96(61)	$Ba_{0.883(14)}Nd_{0.239(9)}Ti_{0.881(13)}O_{3.00(3)}$
0.14	$Ba_{0.86}Nd_{0.28}Ti_{0.86}O_3$	17.18(25)	5.61(15)	17.12(26)	60.09(54)	$Ba_{0.859(13)}Nd_{0.281(8)}Ti_{0.856(13)}O_{3.00(3)}$
0.16*	$Ba_{0.84}Nd_{0.32}Ti_{0.84}O_3$	17.21(29)	5.64(14)	17.13(25)	60.02(61)	$Ba_{0.861(15)}Nd_{0.282(7)}Ti_{0.857(13)}O_{3.00(3)}$

* Small amounts of second phases present in this sample.

Table 2. Refined crystallographic data for composition $x = 0.10$

	x	y	z	B_{iso}	Site
Ba1	1/2	1/2	1/2	0.389(19)	0.890(3)
Nd1				0.389(19)	0.110(3)
Ti2	0	0	0	0.95(5)	0.910(3)
Nd2				0.95(5)	0.090(3)
O1	0	0	1/2	1.225(11)*	

$a = 4.04354(4)$ Å
$R_{wp} = 3.80\%$ $R_E = 1.71\%$
O_1 $B_{11} = B_{22} = 1.04(3)$, $B_{33} = 1.63(5)$.

The graph of lattice parameters against composition, Fig. 1, shows that c decreases slightly for low x, then increases rapidly. The a parameter, however, increases with x, slowly at low x then more rapidly as x increases. This may indicate a different substitution mechanism at low x, e.g., perhaps Nd substitutes purely for Ba at low x, causing contraction of the unit cell. It has been reported that at very low levels of doping (1200 ppm) Nd substitutes primarily at the Ba site, particularly in the presence of excess TiO_2 [18], but at higher levels of substitution it is evident from the present study that Nd substitutes at both sites. The ratio c/a is plotted against x for tetragonal samples in Fig. 4(a). For $0 < x < 0.05(1)$, c/a decreases slowly with x, then for $x > 0.06$, c/a decreases more rapidly. The unit cell volume is plotted against x in Fig. 4(b); the volume increases slowly for $0 < x < 0.04$, then more rapidly for $x > 0.05$, leveling off as the limit of the solid solution is reached.

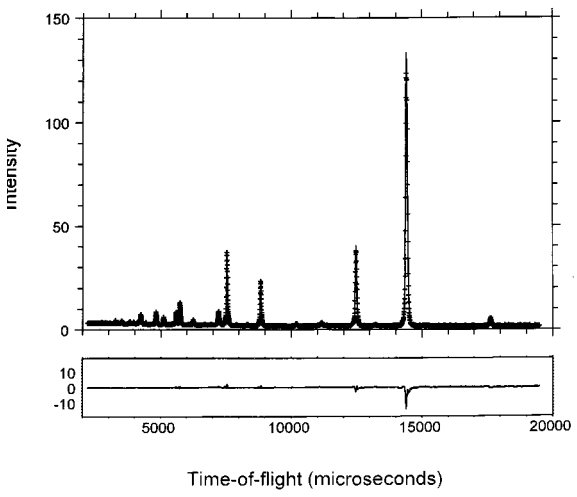

Fig. 3. Observed and difference powder neutron diffraction profile.

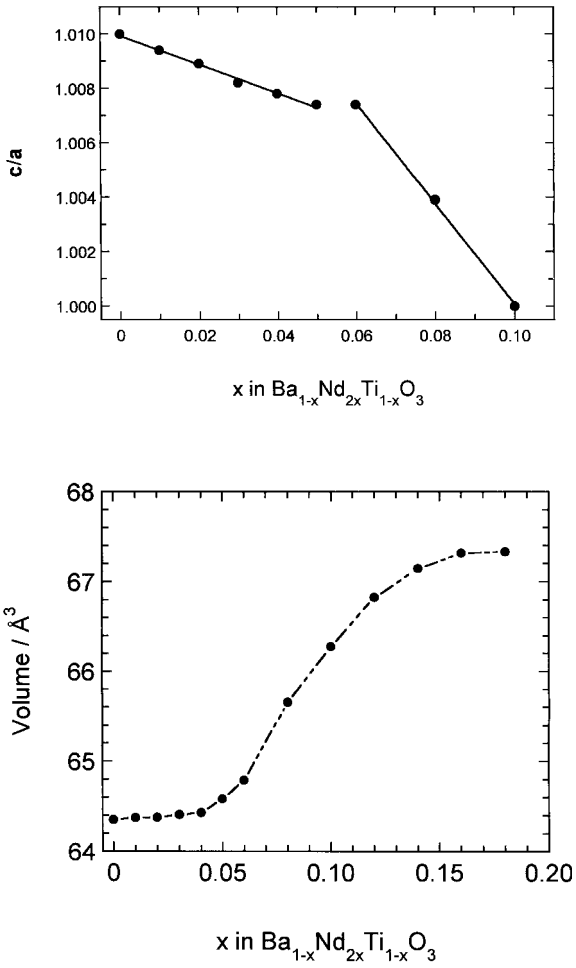

Fig. 4. (a) c/a and (b) V vs. x.

Fixed frequency permittivity data for a range of compositions sintered at 1300°C are shown in Fig. 5. The data show a sharp maximum at 127°C for $x = 0$, in accordance with literature data; with increasing x, the peak broadens rapidly, gradually moves to lower temperatures and finally disappears completely for $x > 0.09$ as the solid solutions become cubic. At intermediate x values, most noticeably at $x = 0.005$ to 0.02, there is evidence for a double maximum in the permittivity against temperature which could represent some inhomogeneity in these compositions even though, macroscopically, the samples appear to be single phase by XRD and EPMA confirmed the homogeneity and phase compositions of the samples at the micron level, Table 1.

Data were also collected for pellets of composition $x = 0.005$, 0.01 and 0.02 which were additionally

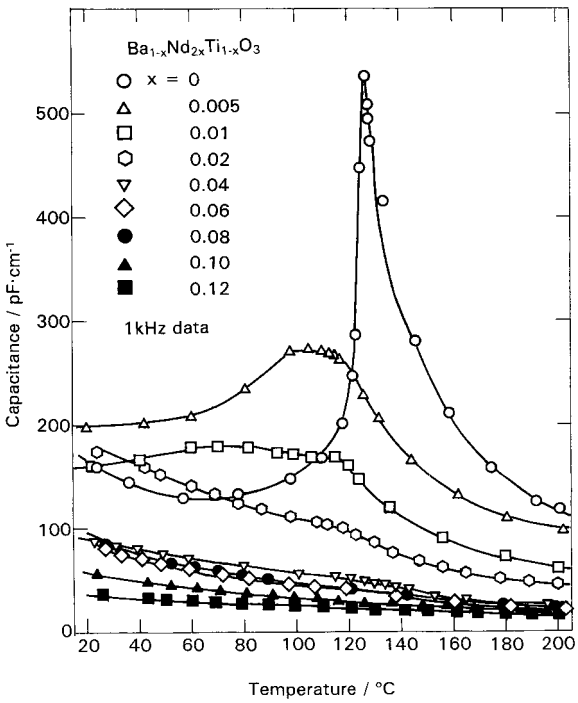

Fig. 5. Permittivity at 1 kHz vs. temperature for different x. Note, permittivity $\varepsilon' = C/e_o$ where $e_o = 8.854 \times 10^{-14} F\,cm^{-1}$.

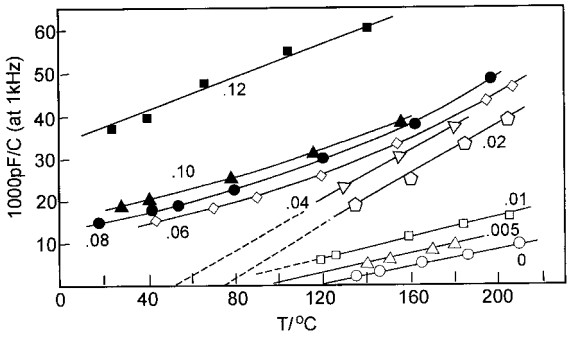

Fig. 6. Curie-Weiss plots for the data presented in Fig. 5, same symbols.

sintered at 1350°C. The permittivity values increased slightly compared with those shown in Fig. 5, but the general behavior was similar, with broad peaks showing evidence of a double maximum. The origin of this double maximum is not known; it is possible that inhomogeneities may exist on a size scale too small to be detected by EPMA and with compositional differences that do not have any significant effect on the XRD patterns.

Curie-Weiss plots of a selection of compositions are shown in Fig. 6; for low x, the extrapolated T_o values gradually decrease with x, from ca. 120°C for $x = 0$ to ca. 60°C for $x = 0.01$. For $x = 0.02$ and 0.04, the Curie-Weiss plot changes slope, but is still linear, with extrapolated T_o values in the range 50 to 70°C. For $x = 0.06$ to 0.10, the behavior changes again and the plots are curved over most of the temperature range. At highest x, 0.12, the Curie-Weiss plot is again linear with a very low extrapolated T_o. These results clearly demonstrate that, at intermediate x values, the electrical behavior of the solid solutions is not simple. At this stage, it is not known whether the solid solutions are inhomogeneous in Nd distribution, whether they exhibit various amounts of cubic and tetragonal phases associated with the diffuse phase transition or whether there is a mixing of the cubic to tetragonal and tetragonal to orthorhombic phase transitions on doping.

The occurrence of broad permittivity maxima is commonly observed in $BaTiO_3$ solid solutions [8,14–17] and again, the broadness may be due to the nature of the diffuse, cubic to tetragonal phase transition; the coexistence of more than one phase in the samples may be observed over a temperature range around the permittivity maximum. It has been reported [8,16,17] that the diffuse nature is due to inhomogeneity or internal stress. In the present case, it is probably caused by the substitution of Nd onto the Ti sites; this inhibits the formation of ferroelectric domains since the relatively large Nd^{3+} ions are likely to be centrally located within the octahedra and do not give rise to individual dipoles. This behavior is in very marked contrast to that observed on La doping [1]. In that case, La substitutes exclusively onto Ba sites, and, although Ti vacancies are created, the ferroelectric domains are preserved, as is the sharp maximum in permittivity vs. temperature. With increasing La content, T_c gradually decreases and the value of ε_{max} increases, reaching $\sim$19000 at 18°C. These two very different cases, involving Nd and La substitution, illustrate the importance of doping mechanisms and the value of combined phase diagram determination, crystallography and electrical property measurement.

Acknowledgments

We thank Dr. A.M. Coats for assistance with the EPMA analysis and Mr. J. Marr for some of the sample preparation.

References

1. F.D. Morrison, D.C. Sinclair, J.M.S. Skakle, and A.R. West, *J. Am. Ceram. Soc*., **81**, 1957 (1998).
2. G.H. Jonker and E.E. Havinga, *Mat. Res. Bull*., **17**, 345 (1982).
3. M. Kahn, *J. Am. Ceram. Soc*., **54**, 455 (1971).
4. J.P. Bonsack, *Am. Ceram. Soc. Bull*., **50**, 488 (1971).
5. K.S. Mazdiyasni and L.M. Borwn, *J. Am. Ceram. Soc*., **54**, 539 (1971).
6. N.M. Molokhia, M.A.A. Issa, and S.A. Nasser, *J. Am. Ceram. Soc*., **67**, 289 (1984).
7. K.S. Mazdiyasni, *Am. Ceram. Soc. Bull*., **63**, 591 (1984).
8. P. Murugaraj, T.R.N. Kutty, and M.S. Rao, *J. Mat. Sci*., **21**, 3521 (1986).
9. C. Zheng and A.R. West, *Brit. Ceram. Proc*., **49**, 247 (1992).
10. T.R.N. Kutty and P. Murugaraj, *J. Mat. Sci*., **22**, 3652 (1989).
11. A.S. Shaikh and R.W. Vest, *J. Am. Ceram. Soc*., **69**, 689 (1986).
12. R.I. Smith and S. Hull, Report RAL-TR-97-038, Rutherford Appleton Laboratory (1997).
13. W.I.F. David, R.M. Ibberson, and J.C. Mathewman, Report RAL-92-032, Rutherford Appleton Laboratory (1992).
14. G. Goodman, *J. Am. Ceram. Soc*., **43**, 105 (1960).
15. D. Barb, E. Barbulescu, and A. Barbulescu, *Phys. Status. Solidi*, **74a**, 79 (1982).
16. D. Hennings, A. Schnell, and G. Simon, *J. Am. Ceram. Soc*., **65**, 539 (1982).
17. H-Y. Lu, J-S. Bow, and W-H. Deng, *J. Am. Ceram. Soc*., **73**, 3562 (1990).
18. K. Takada, E. Chang, and D.M. Smyth, *Adv. in Ceramics*, **19**, 147 (1987).